Chapter 2
Theory of Anomalous Magnetic Dipole Moments of the Electron

Masashi Hayakawa

Abstract The anomalous magnetic dipole moment of the electron, the so-called electron $g-2$, provides us with a high-precision test of quantum electrodynamics (QED), which is the relativistic and quantum-mechanical generalization of electromagnetism, and helps to determine the value of the fine structure constant α, one of the fundamental physical constants. This article intends to give a pedagogical introduction to the theory of $g-2$, in particular, the computation of high-order quantum electrodynamics in $g-2$.

2.1 Introduction

A single electron is known to become magnetized due to its intrinsic charge and spin. Its magnetic dipole moment is given by

$$\boldsymbol{\mu} = -g_e \frac{e\hbar}{2m_e c}\,\mathbf{s}\,, \tag{2.1}$$

where m_e and $\mathbf{s}$ denote the mass and spin of an electron, respectively. The constant g_e represents the strength of the magnetic dipole moment in units of the Bohr magneton, and is called the g-factor of the electron.

At the zeroth order of perturbation, QED predicts that g_ψ is equal to 2 for every massive particle ψ with spin $\frac{1}{2}$. The quantum correction in general shifts g_ψ from 2, depending on the particle species ψ. It is thus convenient to focus on this shift, called the 'anomalous magnetic dipole moment', by introducing a symbol

M. Hayakawa (✉)
Department of Physics, Nagoya University, 464-8602 Nagoya, Japan
e-mail: hayakawa@eken.phys.nagoya-u.ac.jp

W. Quint and M. Vogel (eds.), *Fundamental Physics in Particle Traps*,
Springer Tracts in Modern Physics 256, DOI: 10.1007/978-3-642-45201-7_2,

$$a_\psi \equiv \frac{g_\psi - 2}{2} . \tag{2.2}$$

We shall call this quantity $g-2$ of ψ hereafter.

An important point to notice is the fact that the electron $g-2$, a_e, can be measured very accurately. The most accurately measured value of the electron $g-2$

$$a_e(\mathrm{HV08}) = 1\ 159\ 652\ 180.73\ (28) \times 10^{-12} , \tag{2.3}$$

where the numerals in the parenthesis represent the uncertainty in the final few digits, was obtained by the Harvard group using a Penning trap with cylindrical cavity [1, 2]. The uncertainty (2.3) is smaller than the one obtained by Washington university group in 1987 [3] by a factor 15. See the previous chapter by Gabrielse et al. for a detailed explanation about how such a large reduction of uncertainty has been achieved.

Even if $g-2$ is measured very accurately, one may wonder what physical implication it possesses. Worthy of note is the fact that a_ψ is a predictable quantity in so far as the theory is renormalizable in the framework of quantum field theory. (Section 2.2 introduces the notion and the foundation of the quantum field theory for the readers not specialized in particle physics.) We are thus inclined to question the validity of a renormalizable model of elementary particles by asking the compatibility of its theoretical prediction $a_\psi(\mathrm{th})$ with the experimentally measured value $a_\psi(\mathrm{exp})$.

The *standard model* of elementary particles has endured most of tests for these forty years. It is a renormalizable theory and thus gives a prediction to $g-2$, referred hereafter as $a_\psi(\mathrm{SM})$. The measured value $a_\psi(\mathrm{exp})$ in the experiment may contain the potential contribution $a_\psi(\mathrm{new})$ from the structures which are not built in the standard model

$$a_\psi(\mathrm{exp}) = a_\psi(\mathrm{SM}) + a_\psi(\mathrm{new}) . \tag{2.4}$$

One's actual interest is the existence of such new structures, and its effect on $g-2$ of ψ. Nevertheless, in order to explore its existence through the study of $g-2$, it is indispensable to compute all relevant dynamics of the standard model contributing to $a_\psi(\mathrm{SM})$, and ask if the difference, $a_\psi(\mathrm{exp}) - a_\psi(\mathrm{SM})$, is not zero within available precision.

As is elucidated in full detail in Table 2.1, all the contributions relevant to $a_\mu(\mathrm{SM})$ can be classified unambiguously and exclusively into three components;

Table 2.1 Classification into QED, QCD and weak contributions

Type	Definition
$a_\psi(\mathrm{QED})$	QED with charged leptons[a] only
$a_\psi(\mathrm{QCD})$	(QED + QCD) \(QED with charged leptons only)[b]
$a_\psi(\mathrm{weak})$	All others

[a] All known charged leptons are electron (e), muon (μ) and tau-lepton (τ)

[b] $A \backslash B$ for the sets A and B denotes the intersection of A and the complement of B

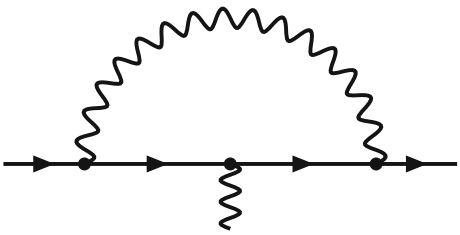

Fig. 2.1 The Feynman diagram giving the lowest-order (second-order) contribution to the anomalous magnetic moment of the lepton

$$a_\psi(\mathrm{SM}) = a_\psi(\mathrm{QED}) + a_\psi(\mathrm{QCD}) + a_\psi(\mathrm{weak})\,. \tag{2.5}$$

The QED contribution $a_\psi(\mathrm{QED})$ is the most dominant among these. For instance, the contribution of the leading order, $O(\alpha)$,[1] of perturbation is induced from the Feynman diagram shown in Fig. 2.1 [4]. (Brief explanation on Feynman diagrams can be found in Sect. 2.2.1.) Figure 2.1, where time flows in the right direction, describes a process in which a single virtual photon is emitted before the lepton ψ couples to the external magnetic field, and is absorbed after that. The theory of $a_\psi(\mathrm{QED})$ is our primary concern in this article.

In Eq. (2.5), $a_\psi(\mathrm{QCD})$ represents the contribution from *QCD*. QCD is the gauge theory of *strong interaction* which binds quarks to form nucleons. Such a contribution arises because every quark has a non-zero electric charge. Figure 2.2 illustrates the QCD contribution to the $g-2$. There, a virtual photon turns into a pair of quark and anti-quark, which receive dynamics of strong interaction and then annihilate into a virtual photon again. $a_\psi(\mathrm{QCD})$ requires evaluation of non-perturbative dynamics of QCD in some manner, and is thus the most difficult to compute. The weak contribution $a_\psi(\mathrm{weak})$ comes from the Feynman diagrams, each of which contains at least one

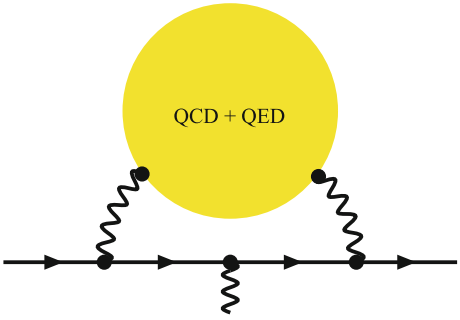

Fig. 2.2 The $O(\alpha^2)$ QCD contribution to the anomalous magnetic moment of the lepton, called the 'leading-order hadronic vacuum polarization contribution', $a_\psi(\mathrm{had.v.p.})$. The blob part denotes the renormalized correlation function $\langle 0|\, T j_\mu^{\mathrm{em}}(x)\, j_\nu^{\mathrm{em}}(y)\,|0\rangle$ of the *hadronic* electromagnetic current j_μ^{em} in QCD + QED

[1] The fine structure constant α is given in terms of the elementary charge e and vacuum permittivity ε_0 by

$$\alpha = \frac{e^2}{4\pi\epsilon_0\hbar c}\,. \tag{2.6}$$

virtual W boson, Z boson or Higgs particle. Section 2.3 explains the basic materials on these non-QED contributions.

Importantly, the sizes of individual contributions on the right hand side of Eq. (2.5) depend sensitively on the mass m_ψ of the species ψ. For larger m_ψ, a_ψ(QCD) and a_ψ(weak) are enhanced relative to a_ψ(QED). Since the muon is heavier than the electron by a factor of about 200, a_μ(QCD), for instance, is about 40,000 times larger than a_e(QCD). Likewise, a_μ(new), the contribution from the as-yet-unknown structures, may also be much larger than a_e(new). This motivates us to study the muon $g-2$ in a serious manner on both sides of experiment and theory, although it is not discussed fully here.

As advocated above, this article intends to give a pedagogical introduction to the QED contribution, a_e(QED), to the electron $g-2$. Section 2.2 provides the generic readers with the introduction of QED, quantum field theory, perturbation theory, and the anomalous magnetic dipole moment in terms of the field theory. Section 2.3 describes the current status of the non-QED contributions. The basic materials of the numerical approach to the computation of high-order QED contributions is explained in Sect. 2.4. Section 2.5 summarizes the latest result for a_e(QED).

2.2 QED and Anomalous Magnetic Dipole Moment

2.2.1 Perturbation Theory of QED

Throughout this article, we work with the natural unit in which the speed of light c and the reduced Planck constant $\hbar$ are set to unity, and with the signature of the metric $\eta^{\mu\nu} = \mathrm{diag}\,(1,\,-1,\,-1,\,-1) = \eta_{\mu\nu}$ with respect to the coordinates $x^\mu = (ct, \mathbf{x})$ in four-dimensional Minkowski space. Einstein convention is employed; the sum over 0, 1, 2, 3 is assumed if the same Greek letter appears twice as a subscript and a superscript in a single term, e.g.,

$$T_{\mu\nu}\,u^\nu \equiv \sum_{\nu=0}^{3} T_{\mu\nu}\,u^\nu\,. \tag{2.7}$$

The classical action of quantum electrodynamics (QED) takes a simple form

$$\begin{aligned} S = \int d^D x \,\Bigg[& -\frac{1}{4}\,F_{\mu\nu}(x)\,F^{\mu\nu}(x) - \frac{1}{2}\left(\partial_\mu A^\mu(x)\right)^2 \\ & + \sum_{\psi=e,\,\mu,\,\tau} \overline{\psi}(x)\left\{\gamma^\mu\left(i\partial_\mu + e\,\mu^{(4-D)/2}A_\mu(x)\right) - m_\psi\right\}\psi(x)\Bigg] \\ & + \text{counter-terms}\,. \end{aligned} \tag{2.8}$$

Several remarks are in order:

1. The field strength $F_{\mu\nu}(x)$ is given in terms of the four-dimensional vector potential $A^{\mu}(x) = (\phi(x),\ \mathbf{A}(x))$, $A_{\mu}(x) \equiv \eta_{\mu\nu}A^{\nu}(x)$ by

$$F_{\mu\nu} = \partial_{\mu}A_{\nu} - \partial_{\nu}A_{\mu} = -F_{\nu\mu}\,. \tag{2.9}$$

$F_{\mu\nu}(x)$ packs the electric field $\mathbf{E}(x)$ and the magnetic field $\mathbf{B}(x)$ in the following manner

$$E^{j}(x) = F^{0j}(x)\ (j = 1,\ 2,\ 3)\,, \quad B^{1}(x) = F_{23}(x) \text{ and cyclic permutation.} \tag{2.10}$$

Through this correspondence, the term bilinear with respect to $F_{\mu\nu}(x)$ in Eq. (2.8) turns out to be the familiar action for the electric and magnetic field

$$\int d^{D}x\ \left(-\frac{1}{4}\,F_{\mu\nu}(x)\,F^{\mu\nu}(x)\right) = \int d^{D}x\,\frac{1}{2}\left(|\mathbf{E}(x)|^{2} - |\mathbf{B}(x)|^{2}\right). \tag{2.11}$$

2. The quantum field theory gives a "unified description of matter and force" in terms of quantum fields. Based on the particle-wave duality in quantum theory, we associate a variable called 'quantum field' to every species from the point of view of a wave. In classical electromagnetism, every component of the vector potential $A_{\mu}(x)$ takes its value in a real number at every space-time point x. After quantization, $A_{\mu}(x)$ becomes a collection of Hermitian operators labelled by $(x,\ \mu)$, and plays the role of creating and annihilating photons, quanta of light. To describe creation and annihilation of one lepton species ψ and its anti-particle, a four-component Dirac field $\left(\psi_{\alpha}(x),\ \overline{\psi}_{\alpha}(x)\right)$ $(\alpha = 1,\ 2,\ 3,\ 4)$ is introduced and promoted to the fields which takes its values in the operators. Gamma matrices γ^{μ} $(\mu = 0,\ 1,\ 2,\ 3)$ are a set of 4×4 matrices satisfying the Clifford algebra corresponding to the signature $\eta^{\mu\nu}$

$$\gamma^{\mu}\gamma^{\nu} + \gamma^{\nu}\gamma^{\mu} = 2\eta^{\mu\nu}\mathbb{I}_{4}. \tag{2.12}$$

3. In Eq. (2.8), the sum is taken over only three leptons, i.e., electron e, muon μ and tau-lepton τ, to focus on the QED contribution in a_{ψ} hereafter.
4. In quantum field theory, the amplitude corresponding to a Feynman diagram in general suffers the divergence due to short-distance singularity (ultra-violet (UV) divergence) and the divergence due to long-distance singularity (infrared (IR) divergence). To regularize these singularities, dimensional regularization is employed, which renders the amplitude well-defined by putting the space-time dimension D away from 0 and all positive integers on the complex plane [5]. A parameter μ with dimension of mass is introduced to keep e dimensionless.

5. The second term in (2.8) is the gauge-fixing term in Feynman gauge.
6. The counter-terms in Eq. (2.8) are treated as the interactions which absorb the divergences emerging from the quantum-mechanical dynamics of the terms in the first integral of Eq. (2.8), Their details will be described in Sect. 2.2.4.

2.2.2 *Feynman Diagrams and Feynman Rule*

Feynman diagrams provide us with a convenient tool to figure all electromagnetic processes relevant to the quantity and the perturbative order of one's interest. In perturbation theory, every term bilinear in fields in the action[2] represents the propagation of a particle (or an antiparticle), while every term trilinear or higher in fields represents the interaction between three or more particles. A Feynman diagram is a graph describing how *virtual* photons, leptons and anti-leptons are created and annihilated in the following way;

1. an undirected wavy line corresponds to the propagation of a free photon,
2. a directed line[3] corresponds to the propagation of a free lepton,
3. a vertex represents the fundamental interaction between lepton and photon.

The Feynman rule [6] derived from the action (2.8) associates the following quantities to a wave line, a directed line and a vertex, respectively where $\not{p} \equiv p_\mu \gamma^\mu$.

$$\Leftrightarrow -\mathrm{i}\frac{\eta^{\mu\nu}}{q^2+\mathrm{i}\varepsilon},$$

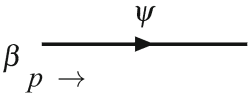

$$\Leftrightarrow \mathrm{i}\frac{\left(\not{p}+m_\psi\right)_{\alpha\beta}}{p^2-m_\psi^2+\mathrm{i}\varepsilon},$$

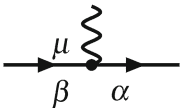

$$\Leftrightarrow \mathrm{i}e\mu^{(4-D)/2}\left(\gamma^\mu\right)_{\alpha\beta},$$

In the graph on the left hand side of the latter equation all lines just guide the eyes, and the quantity on the right hand side is associated with the vertex alone. 'iε with $\varepsilon > 0$' plays the role to specify the boundary condition of Green functions; ε is brought to zero after rotating the zeroth component p^0 of four-momentum to the Euclidean one p_4; $p^0 \to \mathrm{i}p_4$.

The amplitude corresponding to a Feynman diagram is obtained by

---

[2] This applies to the terms except for the counter-terms. All the counter-terms, including bilinear terms, are treated as interactions. See Sect. 2.2.4.

[3] There are actually three types of directed line depending on the species of leptons. See the corresponding Feynman rule (second of the above).

(a) assigning the quantities to the lines or vertices involved in a Feynman diagram,
(b) imposing energy-momentum conservation at every vertex,
(c) integrating n number of independent loop momenta k_r $(r = 1, \ldots, n)$ with

$$\prod_{r=1}^{n} \int \frac{d^D k_r}{(2\pi)^D} \,. \tag{2.13}$$

For instance, a Feynman diagram in Fig. 2.1 gives the amplitude $\mathscr{A}^{\mu}_{\alpha\beta}(p, q)$

$$\begin{aligned} \mathrm{i}\, e\, \mu^{(4-D)/2} \mathscr{A}^{\mu}_{\alpha\beta}(p, q) = \int \frac{d^D k}{(2\pi)^D} \Big[& \mathrm{i}\, e\, \mu^{(4-D)/2}\, \gamma_\lambda \frac{\mathrm{i}}{\not{k} + \not{p} + \not{q}/2 - 1} \\ & \times \mathrm{i}\, e\, \mu^{(4-D)/2}\, \gamma^{\mu} \frac{\mathrm{i}}{\not{k} + \not{p} - \not{q}/2 - 1} \mathrm{i}\, e\, \mu^{(4-D)/2}\, \gamma^{\lambda} \Big]_{\alpha\beta} \\ & \times \frac{-\mathrm{i}}{k^2} \,. \end{aligned} \tag{2.14}$$

Here, q is the four-momentum of the incoming photon, $p \mp q/2$ are the four-momenta of incoming and outgoing external leptons, respectively. The loop momentum is taken to be the momentum k carried by the virtual photon. Since $g - 2$ is a dimensionless quantity, it is convenient to express all dimensionful quantities in units of the mass of the external lepton, parametrizing the effect of creation and annihilation of virtual leptons by *lepton mass ratios*, which appears at the fourth and higher orders. For this reason, the masses in Eq. (2.14) are set to 1. The amplitude (2.14) contains the overall ultra-violet-divergent monopole contribution as well. The contribution to the anomalous magnetic dipole moment from Fig. 2.1 will be obtained by applying the magnetic projection to be discussed in Sect. 2.2.3, to the amplitude (2.14).

For the sake of later reference, the standard technique in quantum field theory to calculate (2.14) is explained here. We can show the identity

$$\frac{1}{ABC} = \frac{1}{2} \int_0^1 dz_1 \int_0^1 dz_2 \int_0^1 dz_a\, \delta\left(1 - (z_1 + z_2 + z_a)\right) \frac{1}{\left(z_a A + z_1 B + z_2 C\right)^3} \,. \tag{2.15}$$

Applying Eq. (2.15) to the integrand of Eq. (2.14) with $A = k^2$, $B = (k+p+q/2)^2 - 1$ and $C = (k + p - q/2)^2 - 1$, and exchanging the order of integration, the integral over the loop momentum k can be easily evaluated.[4] The resulting integral is the one with respect to Feynman parameters z_a, z_1 and z_2.

[4] One can consult with the content of Sect. 2.4.2 on this point.

2.2.3 Anomalous Magnetic Dipole Moment

In this section, we see how the contribution to the anomalous magnetic dipole moment can be extracted from the amplitude in the context of quantum field theory.

Let $\Gamma^{\mu}_{\mathbf{B},\,\alpha\beta}(p,\,q)$ be the unrenormalized vertex function, i.e., the contribution of the one-particle irreducible[5] Feynman diagrams to the Green function

$$\int d^D x_F e^{\mathrm{i}p_F\cdot x_F}\int d^D x_I e^{-\mathrm{i}p_I\cdot x_I}\int d^D y e^{-\mathrm{i}q\cdot y}\,\langle 0|\,\psi_{\mathbf{B},\,\alpha}(x_I)\,j^{\mu}_{\mathrm{em}}(y)\overline{\psi}_{\mathbf{B},\,\beta}(x_F)\,|0\rangle\,, \tag{2.16}$$

where $j^{\mu}_{\mathrm{em}}(x)$ is the electromagnetic current, $p_F = p + \frac{q}{2}$ and $p_I = p - \frac{p}{2}$. The renormalized vertex function $\Gamma^{\mu}_{\alpha\beta}(p,\,q)$ is given in terms of the wave function renormalization constant Z_ψ of the external lepton by

$$\Gamma^{\mu}_{\alpha\beta}(p,\,q) = Z_\psi\,\Gamma^{\mu}_{\mathbf{B},\,\alpha\beta}(p,\,q)\,. \tag{2.17}$$

The invariance of QED under Lorentz-, charge conjugation-(C) and parity (P) transformations as well as the gauge symmetry implies that the renormalized vertex function with the external leptons put on their mass shells, but with the external photon kept off-shell, consists of two form factors $F_1(q^2)$, $F_2(q^2)$[6];

$$\Gamma^{\mu}_{\alpha\beta}(p,\,q)\Big|_{p_F^2=m_\psi^2=p_I^2} = F_1(q^2)\gamma^{\mu} + F_2(q^2)\frac{1}{2m_\psi}\,\mathrm{i}\sigma^{\mu\nu}q_\nu\,, \tag{2.18}$$

where

$$\sigma^{\mu\nu} \equiv \frac{\mathrm{i}}{2}\left[\gamma^{\mu},\,\gamma^{\nu}\right]. \tag{2.19}$$

The on-shell renormalization condition imposes $F_1(q^2 = 0) = 1$ to the electric form factor. The magnetic form factor $F_2(q^2)$ is the quantity predictable in the renormalizable theory. The anomalous magnetic dipole moment is actually identified with $F_2(q^2 = 0)$

$$a_\psi = F_2(0)\,. \tag{2.20}$$

It is an easy exercise to see that a_ψ is obtained by applying the magnetic projection to $\Gamma^{\mu}_{\alpha\beta}(p,\,q)$;

---

[5] A Feynman diagram is called 'one-particle irreducible' if and only if it cannot be divided into two non-trivial connected subdiagrams when any one of the internal lines is cut off.

[6] C and P symmetries are violated in the weak and Yukawa interactions in the standard model, and thus additional form factors are actually induced. However, the classification in Table 2.1 insures that QED and QCD contributions, which respect C and P symmetry, consist of two form factors as in Eq. (2.18).

$$a_\psi = \lim_{q^2\to 0} \frac{m_\psi}{4q^2\left(p^2\right)^2} \mathrm{tr}\left[\left\{m_\psi p^2 \gamma^\mu - \left(m_\psi^2 + \frac{q^2}{2}\right) p^\mu\right\} \times \left(\not{p} + \frac{\not{q}}{2} + m_\psi\right) \Gamma_\mu(p,\, q) \left(\not{p} - \frac{\not{q}}{2} + m_\psi\right)\right], \tag{2.21}$$

with the on-shell conditions $p\cdot q = 0$ and $p^2 + q^2/4 = m_\psi^2$ for the external leptons.

The second-order contribution to a_ψ is obtained by applying (2.21) to $\Gamma^\mu(p,\, q) = \mathscr{A}^\mu(p,\, q)$ in Eq. (2.14) as [4]

$$a_\psi\big|_{\text{1-loop}} = \frac{\alpha}{2\pi}\,. \tag{2.22}$$

2.2.4 Renormalization and Counter-Terms

In perturbation theory of quantum field theory, the notion of counter-terms provides a systematic and practical way to calculate the renormalized amplitude.

The "counter-terms" in (2.8) take the form

$$S_{\text{c.t}} = \int d^D x \left[-\frac{1}{4}\delta Z_A\, F_{\mu\nu}F^{\mu\nu} + \sum_{\psi=e,\,\mu,\,\tau} \left\{\delta Z_\psi\, \overline{\psi}\gamma^\mu i\partial_\mu\psi - \delta Z_{M,\,\psi}\, m_\psi \overline{\psi}\psi + \delta Z_{V,\,\psi}\, e\mu^{(4-D)/2}\overline{\psi}\gamma^\mu A_\mu\psi\right\}\right]. \tag{2.23}$$

and are adjusted to absorb UV divergence. The constants appearing above, δZ_A, δZ_ψ, $\delta Z_{M,\,\psi}$ and $\delta Z_{V,\,\psi}$ are related to the wave function renormalization constants Z_A, Z_ψ, multiplicative mass renormalization constant $Z_{m,\,\psi}$[7] and the coupling renormalization constant Z_e through

$$\delta Z_A = Z_A - 1\,, \quad \delta Z_\psi = Z_\psi - 1\,,$$
$$\delta Z_{M,\,\psi} = Z_\psi Z_{m,\,\psi} - 1\,, \quad \delta Z_{V,\,\psi} = Z_e Z_\psi Z_A^{1/2} - 1\,. \tag{2.24}$$

Perturbatively, the coefficients of counter-terms are expanded in a power series of α/π,

[7] Here we assume that the regularization preserves the non-anomalous chiral symmetry, so that no linear additive UV divergence arises in the two-point functions of leptons.

$$\delta Z_A = \sum_{n=1}^{\infty} \delta^{(n)} Z_A \left(\frac{\alpha}{\pi}\right)^n , \quad \delta Z_\psi = \sum_{n=1}^{\infty} \delta^{(n)} Z_\psi \left(\frac{\alpha}{\pi}\right)^n ,$$
$$\delta Z_{M,\psi} = \sum_{n=1}^{\infty} \delta^{(n)} Z_{M,\psi} \left(\frac{\alpha}{\pi}\right)^n , \quad \delta Z_{V,\psi} = \sum_{n=1}^{\infty} \delta^{(n)} Z_{V,\psi} \left(\frac{\alpha}{\pi}\right)^n . \quad (2.25)$$

These counter-terms generate the *interaction vertices* of various orders of perturbation theory. In particular, the renormalization of wave function or mass corresponds to a vertex from which only two lines emanate. The lower-order counter-terms together with QED interaction generate the Feynman diagrams and the subtraction terms which cancel ultra-violet divergences contained in subdiagrams. In the end, the sum of all those Feynman diagrams can have only *overall UV divergences that should be cancelled by the nth-order coefficients*, $\delta^{(n)} Z_A$, etc. Their precise values are determined from the demand that the renormalized vertex functions, $\Pi(q^2)$, $\Sigma_{\alpha\beta}(p)$ and $\Lambda^\mu(p, q)$, defined by

$$\int d^D x\, e^{iq\cdot x} \langle 0|\, A_\mu(x) A_\nu(0)\, |0\rangle = \frac{-\mathrm{i}\eta_{\mu\nu}}{q^2\left\{1 - \Pi(q^2)\right\}} ,$$
$$\int d^D x\, e^{ip\cdot x} \langle 0|\, \psi_\alpha(x)\overline{\psi}_\beta(0)\, |0\rangle = \left[\frac{\mathrm{i}}{\not{p} - m - \Sigma(p)}\right]_{\alpha\beta} ,$$
$$\Gamma^\mu_{\alpha\beta}(p, q) = \gamma^\mu_{\alpha\beta} + \Lambda^\mu_{\alpha\beta}(p, q) , \quad (2.26)$$

satisfy certain *renormalization conditions*. The gauge symmetry guarantees that Z_e is independent of ψ. In this way, the counter-terms are determined iteratively in perturbation theory of QED.

2.2.5 Classification of Perturbative Dynamics

The quantum electrodynamics in the lepton $g - 2$, $a_\psi(\mathrm{QED})$, are expected to be obtained by computing the coefficients $a_\psi^{(2n)}$ in the perturbative series

$$a_\psi(\mathrm{QED}) = \sum_{n=1}^{\infty} a_\psi^{(2n)} \left(\frac{\alpha}{\pi}\right)^n , \quad (2.27)$$

up to the order N determined from the requirement of experimental accuracy and our theoretical interest. In what follows, the nth term in Eq. (2.27) is called 'n-loop term' or the '$2n$th-order term', as it is $O(\alpha^n) \sim O(e^{2n})$. The comparison of Eq. (2.22) with (2.27) yields the leading-order coefficient $a_\psi^{(2)}$ as

$$a_\psi^{(2)} = \frac{1}{2} \equiv A_1^{(2)} . \quad (2.28)$$

Before starting any calculations, the most dominant contribution should be identified. To do so in our context, we decompose the contributions into four types according to the dependence on lepton mass ratios (Recall the discussion below Eq. (2.14.));

$$a_e^{(2n)} = A_1^{(2n)} + A_2^{(2n)}\left(\frac{m_e}{m_\mu}\right) + A_2^{(2n)}\left(\frac{m_e}{m_\tau}\right) + A_3^{(2n)}\left(\frac{m_e}{m_\mu}, \frac{m_e}{m_\tau}\right). \tag{2.29}$$

Here, the subscript j attached to $A_j^{(2n)}$ denotes the number of leptons involved in its calculation. $A_1^{(2n)}$ is the contribution that should be computed in *QED with electron only*. It is a pure number and called 'mass-independent term', and thus universally contributes to $g-2$ of all leptons ψ. $A_1^{(2)}$ is given by Eq. (2.28). $A_2^{(2n)}\left(\frac{m_e}{m_\mu}\right)$ is the contribution to the electron $g-2$ from all Feynman diagrams with at least one muon loop but with no tau-lepton loop. $A_2^{(2n)}\left(\frac{m_e}{m_\tau}\right)$ is similarly defined. $A_3^{(2n)}\left(\frac{m_e}{m_\mu}, \frac{m_e}{m_\tau}\right)$ is the contribution of all Feynman diagrams with both muon loop(s) and tau-lepton loop(s). $A_2^{(2n)}$ appears at first at the fourth order. $A_3^{(2n)}$ appears at first at the sixth order.

Muon and tau-lepton are both much heavier than the electron. Thus, for the electron $g-2$, their virtual effects are suppressed compared to the dynamics of QED with electron only. Therefore, $A_1^{(2n)}$ is the most dominant at every order $2n$ in the electron $g-2$.

It would be instructive to compare such a perturbative feature of QED in the electron $g-2$ with that in the muon $g-2$. In the similar manner as in (2.29), each coefficient $a_\mu^{(2n)}$ in the perturbative expansion of a_μ(QED) can be decomposed into four types of terms;

$$a_\mu^{(2n)} = A_1^{(2n)} + A_2^{(2n)}\left(\frac{m_\mu}{m_e}\right) + A_2^{(2n)}\left(\frac{m_\mu}{m_\tau}\right) + A_3^{(2n)}\left(\frac{m_\mu}{m_e}, \frac{m_\mu}{m_\tau}\right). \tag{2.30}$$

The meaning of each term would now be obvious from the dependence on lepton mass ratio(s). Since the electron is lighter than the muon, $A_2^{(2n)}\left(\frac{m_\mu}{m_e}\right)$ dominates $a_\mu^{(2n)}$ for $2n \geq 6$.

2.3 Non-QED Contribution to $g-2$

The standard model contribution was decomposed into three parts as in Eq. (2.5). Table 2.2 summarizes the results for the non-QED contribution to the electron $g-2$ obtained thus far. In that table, the last one is the weak contribution, and the others are the QCD contributions relevant to the precision of our interest. Table 2.2 also

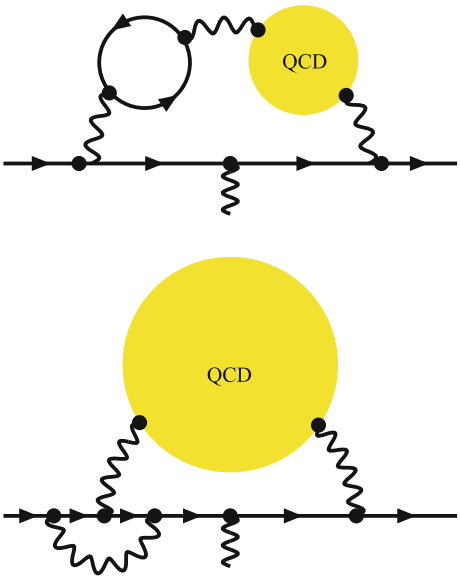

Fig. 2.3 Examples of the next-to-leading-order ($O(\alpha^3)$) hadronic vacuum polarization contribution, a_ψ(NLO had.v.p.), to the anomalous magnetic dipole moment

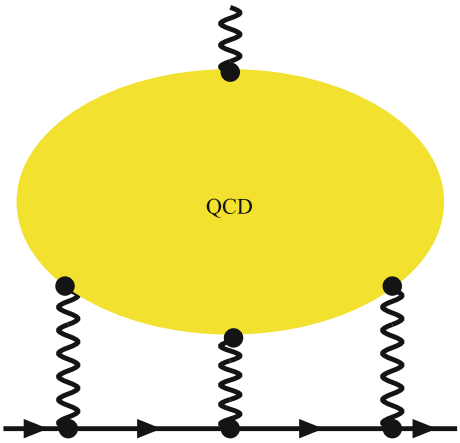

Fig. 2.4 Hadronic light-by-light scattering contribution a_ψ(had.l-l)

shows that they are only small part of a_e, but can no longer be neglected compared to the current experimental accuracy (2.3). Below we focus on the QCD contribution.

The QCD contributions relevant to the electron $g-2$ in view of the experimental accuracy are represented by the diagrams shown in Figs. 2.2, 2.3 and 2.4, and a_e(QCD) is given by their sum

$$a_e(\text{QCD}) = a_e(\text{had.v.p.}) + a_e(\text{NLO had.v.p.}) + a_e(\text{had.}l\text{-}l)\,. \tag{2.31}$$

Here, $O(\alpha^2)$-hadronic vacuum polarization contribution, a_e(had.v.p.), corresponds to the diagram in Fig. 2.2. Note that it also includes the $O(\alpha^3)$-terms caused by a

single virtual photon exchange between quarks in the blob part. The QED correction to a photon line, lepton line or leptonic vertex in Fig. 2.2 gives rise to the next-to-leading-order (NLO) hadronic vacuum polarization contribution, a_e(NLO had.v.p.). Figure 2.3 illustrates a Feynman diagram contributing to a_e(NLO had.v.p.). Lastly, the hadronic light-by-light scattering contribution shown in Fig. 2.4, a_e(had.*l-l*), is also the order of α^3, and is induced through the elastic scattering between two photons *caused by QCD*.

Since the strongly coupled dynamics at low energy $\lesssim$1 GeV is the most important to the electron $g-2$, perturbation theory of QCD cannot account for the bulk contribution to the lepton $g-2$. In general, we must rely on some numerical means to capture the non-perturbative dynamics of QCD. For the hadronic vacuum polarization type contributions, i.e., a_ψ(had.v.p.) and a_ψ(NLO had.v.p.), we can circumvent direct computation of non-perturbative QCD dynamics as follows. The dispersive expression for the vacuum polarization function and the optical theorem, which follows from the unitary of S matrix, enables to express a_ψ(had.v.p.) as the convolution of R ratio $\widehat{R}(s)$, where $\sqrt{s} = 2E_{\rm cm}$ for the electron energy $E_{\rm cm}$ in the center of mass frame of the electron and positron beams, and a calculable function $K(s)$

$$a_\psi(\text{had.v.p.}) = \left(\frac{\alpha}{3\pi}\right)^2 \int_{E_{\rm th}^2}^{\infty} \frac{ds}{s} \frac{m_\psi^2}{s} \widehat{R}(s)\, K(s)\,, \tag{2.32}$$

with $E_{\rm th} = m_{\pi^0}$. The function $K(s)$ increases from 0.4 at $E_{\rm th}$ monotonically and approaches to 1 for $s \to \infty$. (The explicit expression of $K(s)$ is available, e.g. in [7].) To take the $O(\alpha)$ QED correction to the blob part in Fig. 2.2 into account, we focus on the the cross section $\sigma_h(s)$ in the unpolarized e^+e^- collision with the hadrons or hadrons $+\gamma$ as the final states, but with no initial state photon radiation. Note that the R ratio $\widehat{R}(s)$ required in Eq. (2.32) is not the experimentally accessible quantity $\sigma_h(s)$, but $\widehat{\sigma}_h(s)$ which is obtained from $\sigma_h(s)$ by removing $O(\alpha)$ correction to the part $e^+e^- \to \gamma^*$

$$\widehat{R}(s) = \frac{\widehat{\sigma}_h(s)}{\frac{4\pi\alpha^2}{3s}}\,. \tag{2.33}$$

The additional QED correction residing in $\sigma_h(s)$ compared to $\widehat{\sigma}_h(s)$ is exactly the charge renormalization. Therefore, these two quantities are related as

$$\widehat{\sigma}_h(s) = \left(\frac{\alpha}{\alpha(s)}\right)^2 \sigma_h(s)\,, \tag{2.34}$$

where, for the relevant order of α, $\sigma(e^+e^- \to \gamma^* \to \text{hadrons})$ only suffices for the QCD effect in the running gauge coupling constant $\alpha(s)$. a_ψ(NLO had.v.p.) can also be obtained with use of $\sigma(e^+e^- \to \gamma^* \to \text{hadrons})$ and the different function for $K(s)$.

Table 2.2 Summary of non-QED contribution to the electron $g-2$

Contribution X	$X \times 10^{12}$	Reference
a_e(had.v.p.)	1.866(12)	[9]
a_e(NLO had.v.p.)	−0.2234(14)	[9]
a_e(had.l-l)	0.035(10)	[10]
a_e(weak)	0.0297(5)	[11–14]

The first three are QCD contributions. a_e(weak) is estimated by scaling a_μ(weak) with the electron-muon mass ratio took into account

Practically, an inclusive cross section is impossible to directly measure; it is actually obtained by summing up all relevant exclusive cross sections. Experimental papers have reported their results for the individual cross section with or without radiative corrections, and thus careful treatment is necessary to gather and compile various data [8].

In contrast to the vacuum-polarization-type contribution, the hadronic light-by-light scattering contribution has not been successfully expressed in terms of some experimentally accessible quantities, and thus it requires explicit theoretical computation of non-perturbative QCD dynamics. The computation of this quantity is one of the remained subjects of the lepton $g-2$, in particular, the muon $g-2$. Thus far, it has been mostly evaluated according to the low-energy effective theory of QCD and/or hadronic models. a_e(had.l-l) in Table 2.2 was also obtained in this manner [10]. Even though its order in Table 2.2 is found to be much smaller than the one of our interest, it should be calculated by some other method.

2.4 Numerical Approach to Perturbative QED Calculation

The perturbative coefficients $a_\psi^{(2n)}$ have been known exactly or as an expansion in power series of mass ratios for $n = 1,\ 2,\ 3$. (See Sect. 2.5 for the literature concerning with the lower-order coefficients.) The eighth-order coefficient $a_\psi^{(8)}$ and the tenth-order coefficient $a_\psi^{(10)}$ [15–24], however, have been evaluated only by numerical means. Here, a succinct explanation is given for a particular method adopted to compute $a_\psi^{(8)}$ and $a_\psi^{(10)}$. The reader who would like to know full details on the parametric integral formalism, in particular on the ways of construction of ultraviolet and infrared subtraction terms can consult with the review article [25] or the original references [26–29].

2.4.1 Classification of Feynman Diagrams

Here we see the scheme of classification of Feynman diagrams employed in a series of works [15–24].

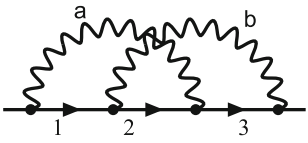

Fig. 2.5 A self-energy-like Feynman diagram (4a) corresponding to three vertex-type diagrams giving the fourth-order contribution to the anomalous magnetic moment of the lepton

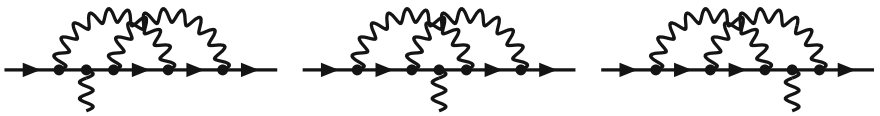

Fig. 2.6 The vertex diagrams at the fourth order related to a self-energy-like diagram in Fig. 2.5 via Ward-Takahashi identity (2.35)

We start with introducing the notion of *self-energy-like* (Feynman) diagram. A self-energy-like diagram is a diagram obtained from a vertex diagram by removing the external vertex. Note that the contribution to the self-energy function from a self-energy-like diagram may vanish identically. Such an example is the sixth-order light-by-light scattering diagram, where the external vertex lies on the virtual lepton loop. Note also that two different vertex diagrams are possibly reduced to the same self-energy-diagram if the external vertices are removed.

The reason why we focus on self-energy-like diagrams in place of vertex diagrams is based on the following important but unfamiliar fact; the Ward-Takahashi (WT) identity, which results from the gauge invariance of the system, holds between the contribution to the self-energy function $\Sigma(p)$ from a single self-energy-like Feynman diagram $\mathcal{G}$ and the contribution to the vertex function $\Lambda^{\mu}(p,\, q)$ from a set $\mathcal{B}_{\mathcal{G}}$ of vertex diagrams which can be obtained by inserting a single QED vertex into one of the lepton lines on the open path connected to the initial and final leptons, or the loop with odd number of internal vertices in all possible ways;

$$\sum_{\mathcal{V}\in\mathcal{B}_{\mathcal{G}}} q_{\nu}\Lambda^{\nu}_{\mathcal{V}}(p,\, q) = -\Sigma_{\mathcal{G}}\left(p+\frac{q}{2}\right) + \Sigma_{\mathcal{G}}\left(p-\frac{q}{2}\right). \tag{2.35}$$

For instance, to the self-energy function $\Sigma_{\mathcal{G}}$ from a single self-energy-like diagram $\mathcal{G}$ in Fig. 2.5, the sum of contributions to the vertex functions from three diagrams in Fig. 2.6 are related through Eq. (2.35).

By differentiating both sides of Eq. (2.35) with respect to the incoming photon momentum q_{μ}, and taking the limit $q \to 0$, we find

$$\sum_{\mathcal{V}\in\mathcal{B}_{\mathcal{G}}} \Lambda^{\mu}_{\mathcal{V}}(p,\, q\simeq 0) \simeq \sum_{\mathcal{V}\in\mathcal{B}_{\mathcal{G}}} \left\{ -q_{\nu}\left[\frac{\partial\Lambda^{\nu}_{\mathcal{V}}(p,\, q)}{\partial q_{\mu}}\right]_{q=0}\right\} - \frac{\partial\Sigma_{\mathcal{G}}(p)}{\partial p_{\mu}}. \tag{2.36}$$

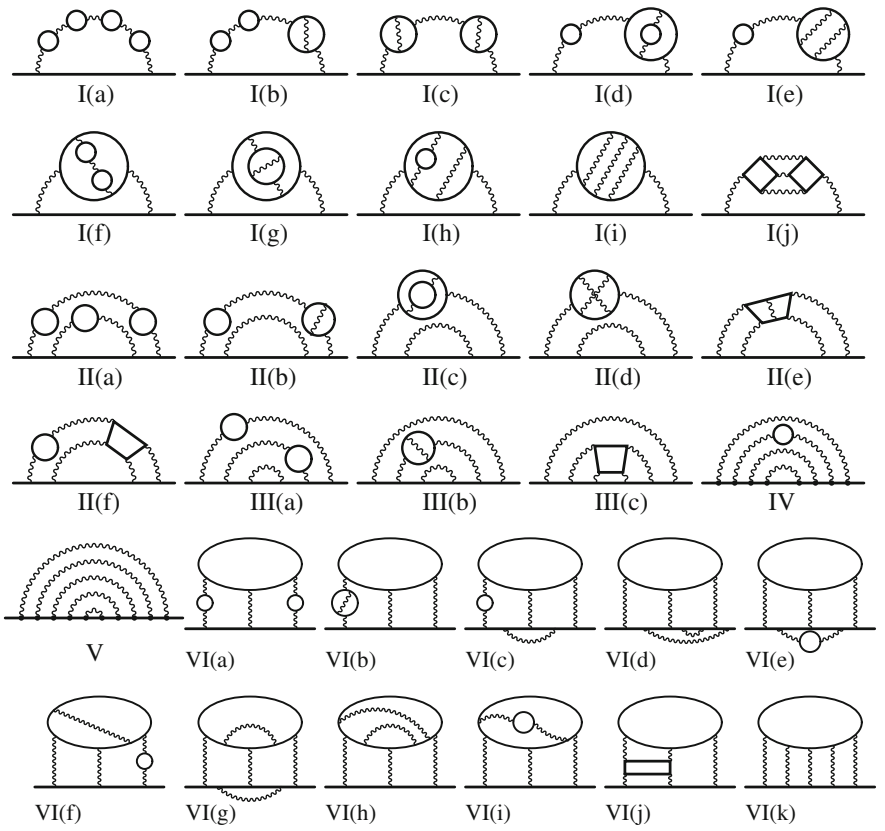

Fig. 2.7 Gauge-invariant subsets of self-energy-like diagrams at the tenth order

Via this identity, it is possible to obtain the expression of *the sum* $M_{\mathcal{G}}$ *of the bare amplitudes of* $g-2$ *induced from the vertex diagrams in* $\mathcal{B}_{\mathcal{G}}$ *which are related to a single self-energy-diagram* $\mathcal{G}$ simultaneously, once we find the expression of the integrand for the bare Feynman amplitude of $\Sigma_{\mathcal{G}}(p)$ in the momentum space.

Moreover, all the vertex diagrams belonging to $\mathcal{B}_{\mathcal{G}}$ have similar ultra-violet (UV) and infrared (IR) divergent structures, as we will see this point explicitly within the parametric integral formalism in Sect. 2.4.3. Since the number of self-energy-like diagrams is much smaller than that of the vertex diagrams by the factor $1/(2n-1)$, we first categorize the vertex diagrams at the order of our interest into the sets represented by the corresponding self-energy-like diagrams. We next classify the self-energy-like diagrams into the minimal gauge-invariant subsets. Note that a gauge-invariant set means the set of diagrams whose sum of contributions is independent of the choice of gauge fixing condition. The minimal gauge-invariant subsets can be immediately identified if one's attention is paid to the types and the number of lepton loops involved. This point can be seen in Fig. 2.7, which lists up all the gauge-invariant subsets for the self-energy-like diagrams at the tenth order [15, 28].

2.4.2 Parametric Representation of Feynman Diagrams

As introduced in Sect. 2.2.1, the amplitude can be expressed as an integral of Feynman parameters. Here, we overview a way to write down the bare amplitude in terms of building blocks which will turn out to help to construct the terms cancelling the ultra-violet and infrared divergences on the Feynman parameter space.

For that purpose, we return to Eq. (2.14), and overview the standard calculational method of the Feynman amplitude. The numerator of the integrand of Eq. (2.14) involves

$$\left\{\not{k}+\not{p}+\frac{\not{q}}{2}+1\right\}\otimes\left\{\not{k}+\not{p}-\frac{\not{q}}{2}+1\right\}, \tag{2.37}$$

which can be written in terms of $k = l - z_1\left(p+\frac{q}{2}\right) - z_2\left(p-\frac{q}{2}\right)$ with new loop momentum l as

$$\begin{aligned} f\ &\left\{\not{l}+(1-z_1)\left(\not{p}+\frac{\not{q}}{2}\right)-z_2\left(\not{p}+\frac{\not{q}}{2}\right)+1\right\} \\ &\otimes\left\{\not{l}-z_1\left(\not{p}+\frac{\not{q}}{2}\right)+(1-z_2)\left(\not{p}-\frac{\not{q}}{2}\right)+1\right\}. \end{aligned} \tag{2.38}$$

Now that the denominator is an even function of l, the terms with odd number of l in the numerator all vanish upon loop integration. Thus, the integral consists of two types

$$\int\frac{d^Dl}{(2\pi)^D}\,\frac{l_\mu l_\nu}{\left\{l^2-C(z_1,\,z_2)+i\varepsilon\right\}^3}\,,\quad \int\frac{d^Dl}{(2\pi)^D}\,\frac{1}{\left\{l^2-C(z_1,\,z_2)+i\varepsilon\right\}^3}\,, \tag{2.39}$$

which can be performed easily.

Even at higher order of perturbation, the manipulation to write down the amplitude as an integral on Feynman space is essentially the same. In practice, however, it needs such devises that realize

(1) construction of the bare amplitude can be systematically done,
(2) construction of the terms to *numerically subtract* ultra-violet divergence and infrared divergence can be done systematically.

The parametric integral formalism provides a method to calculate the perturbative coefficients numerically with the properties (1) and (2). There, the numerical calculation is done on the Feynman parameter space. The loop momenta $\{k_r\}_{r=1,\cdots,n}$ (n is the total number of loops.) must thus be carried out manually. To do so, we first convert n_I number of the denominators of propagators (n_I denotes the number of internal lines in the diagram) to a single denominator through the formula

$$\prod_{j=1}^{n_I} \frac{1}{H_i} = (n_I - 1)! \prod_{j=1}^{n_I} \int_0^1 dz_j \, \delta\left(1 - \sum_{k=1}^{n_I} z_k\right) \frac{1}{\left(\sum_{i=1}^{n_I} z_i H_i\right)^{n_I}}. \tag{2.40}$$

Next, we pull out the momenta p_i appearing in the numerators of lepton propagators outside of the loop integrals by replacing p_i by the D operator

$$D_i^\mu \equiv \frac{1}{2} \int_{m_i^2}^\infty dm_i^2 \, \frac{\partial}{\partial q_{i,\mu}}, \tag{2.41}$$

where we decompose $p_i = k_i + q_i$ into the linear combination k_i of loop momenta k_r and the combination q_i of the external momenta. The amplitude of, say, a vertex diagram $\mathscr{G}$ with no lepton loop can be written as[8,9]

$$\begin{aligned}
\Gamma_{\mathscr{G}}^{\nu} &= \left(-\frac{1}{4}\right)^n (n-1)! \, \mathbb{F}^\nu \int (dz)_{\mathscr{G}} \, \frac{1}{U^2 \, V^n}, \\
(dz)_{\mathscr{G}} &\equiv \prod_{j=1}^{n_I} dz_j \, \times \delta\left(1 - \sum_{i=1}^{n_I} z_i\right), \\
V &\equiv \sum_{i=1}^{n_I} z_i \left(m_i^2 - q_i \cdot Q_i'\right), \\
Q_j'^{\mu} &\equiv -\frac{1}{U} \sum_{i=1}^{n_I} q_i^\mu z_i \, B_{ij}', \quad B_{ij}' \equiv B_{ij} - \delta_{ij} \frac{U}{z_j}.
\end{aligned}$$

$$\mathbb{F}^\nu = \gamma^{\alpha_1} (\not{p}_1 + m_1) \, \gamma^{\alpha_2} \cdots \gamma^{\nu} \cdots \gamma^{\alpha_{2n-1}} (\not{p}_{2n} + m_{2n}) \, \gamma^{\alpha_{2n}} \prod_{k=1}^{n} \eta_{\alpha_{i_k} \alpha_{j_k}}. \tag{2.42}$$

U and B_{ij} are functions of Feynman parameters, and are determined by the *chain topology* of the diagram $\mathscr{G}$.

A *chain* is a set of consecutive internal lines with their types disregarded, which are connected by the external vertices only. A chain may consist of a single internal line, or of the internal lepton and photon lines (e.g., $\{1, a\}$ in Fig. 2.5). The chain diagram of $\mathscr{G}$ is a "vacuum diagram" consisting of the chains and the internal vertices of $\mathscr{G}$. For example, Fig. 2.8 shows the chain diagram of *all* vertex-type diagrams in Figs. 2.5 and 2.6 . One immediately understands that all vertex-type diagrams related

[8] We set $D = 4$ to simplify the expression.

[9] Diagrams with no lepton loop, called 'quenched-type diagrams', are completely described by a set of pairing of lepton indices $\{(i_k, j_k)\}_{k=1,\ldots,n}$ ($i_k < j_k$, $i_1 < \cdots < i_n$ and $j_{k_1} \neq j_{k_2}$ for $k_1 \neq k_2$.).

via the WT-identity to a self-energy-like diagram share a common chain diagram, in general.

For a non-self-intersecting loop $\mathscr{C}$, we introduce the incident matrix $\{\xi_{c,\mathscr{C}}\}$ associated with the chain topology of $\mathscr{G}$

$$\xi_{c,\mathscr{C}} = \begin{cases} 1 & \text{if } c \in \mathscr{C} \text{ and chain } c \text{ has the same direction as } \mathscr{C} \\ -1 & \text{if } c \in \mathscr{C} \text{ and chain } c \text{ has the direction opposite to } \mathscr{C} \\ 0 & \text{if } c \notin \mathscr{C} \end{cases} . \tag{2.43}$$

Accordingly, we assign the Feynman parameter z_c to the chain c as

$$z_c = \sum_{j \in c} z_j \, . \tag{2.44}$$

In Figs. 2.5 and 2.8,

$$z_{c_1} = z_1 + z_a \, , \quad z_{c_2} = z_2 \, , \quad z_{c_3} = z_3 + z_b . \tag{2.45}$$

Starting with $U = z_c$ for a loop (the chain topology of the one-loop diagram), B_{c_1,c_2} and U are obtained recursively according to the following equations

$$\begin{aligned} B_{c_1,c_2} &= \sum_{\mathscr{C}} \xi_{c_1,\mathscr{C}} \xi_{c_2,\mathscr{C}} U_{\mathscr{G}/\mathscr{C}} \, , \\ \xi_{c,\mathscr{C}_0} U &= \sum_{c'} \xi_{c',\mathscr{C}_0} z_{c'} B_{c',c} \, . \end{aligned} \tag{2.46}$$

Here, $\mathscr{G}/\mathscr{C}$ denotes the reduced diagram which is obtained by shrinking $\mathscr{C}$ to a single vertex in $\mathscr{G}$. $\mathscr{C}_0$ and c in the second equation are arbitrarily chosen loop and a chain on it, respectively. Equation (2.46) shows that B_{c_1,c_2} and U are functions of Feynman parameters of homogeneous degrees $n-1$ and n, respectively. $B_{ij} = B_{ji}$ for a pair of the internal lines i, j is equal to $+B_{c_1,c_2}$ for $i \in c_1$, $j \in c_2$ if both lines have the same or the opposite directions as the chains, and to $-B_{c_1,c_2}$ otherwise.

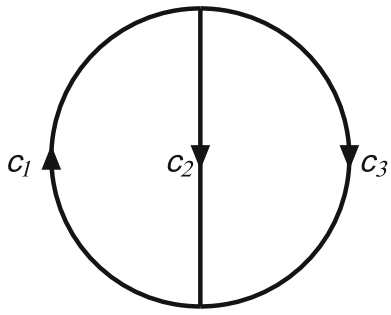

Fig. 2.8 Chain diagram of the fourth-order Feynman diagram (4a)

For the chain diagram in Fig. 2.8,

$$B_{c_1,\,c_2} = z_{c_2} + z_{c_3}, \quad B_{c_2,\,c_1} = z_{c_3}, \tag{2.47}$$

and we have for the choice $c = c_1$ and $\mathscr{C}_0 = \{c_1,\, c_2\}$ in the second equation of Eq. (2.46)

$$U = z_{c_1} B_{c_1,\,c_1} + z_{c_2} B_{c_2,\,c_1} = z_{c_1} z_{c_2} + z_{c_2} z_{c_3} + z_{c_3} z_{c_1}\,. \tag{2.48}$$

The application of D operators contained in $\mathbb{F}^\nu$ of Eq. (2.42) will yield the terms as in Eq. (2.39). It is straightforward to see that the manipulation of D operators is equivalent to performing all possible ways of following *contraction operations*:

(a) In case that D_i^μ and D_j^ν are "contracted", they are turned into $\left(-\frac{1}{2}\, B'_{ij}\, \eta^{\mu\nu}\right)$.
(b) The uncontracted D_i^μ is replaced by $Q_i'^{\,\mu}$.
(c) The terms obtained by k-time contraction is multiplied by

$$\frac{1}{(n-1)\cdots(n-k)}\,\frac{1}{U^{k+2}\,V^{n-k}}\,, \tag{2.49}$$

in place of $\dfrac{1}{U^2 V^n}$.

The denominator of the resulting integrand is now written in terms of B_{ij} and $Q_i'^{\,\mu}$. A vectorial quantity $Q_i'^{\,\mu}$ is expressed as a linear combination of the external momenta with the *scalar currents* A_i^p, A_i^q as the coefficients

$$Q_i'^{\,\mu} = A_i^p\, p^\mu + A_i^q\, q^\mu\,. \tag{2.50}$$

(See the explanation just below Eq. (2.14) for the meaning of $p,\ q$.) No A_i^q appears in the expression of the integrand of $g-2$ amplitude. A_i^p is given in terms of B'_{ij} and U as [27]

$$A_i^p = -\frac{1}{U}\sum_{j=1}^{n_I} \eta_{j,\,\mathscr{P}}\, z_j\, B'_{ji}\,, \tag{2.51}$$

for the path $\mathscr{P}$ consisting of all consecutive lepton lines connected to the external leptonic states, and $\eta_{j,\,\mathscr{P}}$ is 1 (-1) if the line j lies on $\mathscr{P}$ with the same (opposite) direction, and 0 otherwise.

Obviously, use of U, B_{ij} and A_i^p as "building blocks" of the integrand[10] reduces the size of the expression of the integrand, compared to the one written solely in

[10] The WT-summed amplitude consists of four types of terms. One is written by

$$\widetilde{C}_{ij} = \frac{1}{U}\sum_{k<l} z_k z_l \left(B'_{ik}B'_{jl} - B'_{il}B'_{jk}\right)\,, \tag{2.52}$$

terms of $\{z_i\}$, and thus reduces the computational cost significantly. Furthermore, it will turn out that they also play the essential role in the systematic construction of the integrands of the terms to subtract divergence. In order to see a little bit about this point, we end this section with observing when ultra-violet (UV) divergence and infrared (IR) divergence can arise. From Eq. (2.51), it turns out that the scalar currents are rational functions of Feynman parameters with homogeneous degree 0. Thus, V in Eq. (2.42) is a rational function with homogeneous degree 1. Hence, the terms obtained by the same number of contractions, whose integrands are all proportional to the quantity (2.49), have the same homogeneous degree. Note that the terms obtained by more and more number of contraction operations correspond to the ones with more and more loop momenta in the numerators of the integrands, and thus become dominated by larger and larger momenta. As seen in Eq. (2.49), contraction increases the degree of U while it decreases that of V in the denominator. Hence, UV divergences can arise on some boundary of Feynman parameter space where $U \to 0$. Likewise, IR divergences can arise where $V \to 0$.

2.4.3 Subtraction of UV and IR Divergences

One of the distinguishing features of the numerical method [26–29] adopted to compute the high-order QED contribution to a_ψ is the *numerical subtraction* of ultra-violet (UV) divergences in the Feynman amplitudes. We suppose that those amplitudes are written in the form of the parametric integrals, as was explained in Sect. 2.4.2.

The numerical subtraction of divergence can be attained only if the bare amplitude and all the required subtraction terms are prepared on the common Feynman parameter space, and singularities are organized to be cancelled in a pointwise way. This way of singularity cancellation, however, requires that a single vertex-type Feynman diagram, or some set of vertex-type Feynman diagrams sharing a common UV structure must be dealt with separately to prepare the subtraction terms. Here we start with observing that a collection of vertex subdiagrams associated with one self-energy-like diagram is a reasonable example of such sets.

As already remarked, the definition of a self-energy-like diagram in Sect. 2.4.1 and the definition of the chain in Sect. 2.4.2 implies that a collection of vertex-type Feynman diagrams related to a given self-energy-like diagram shares the same chain topology. Therefore, those vertex-type diagrams share common U and B_{ij}. Since UV subdivergence appears on the boundary of Feynman parameter space where U vanishes, these diagrams have the same UV divergent structure.

As already mentioned above, the use of the Ward-Takahashi (WT) identity (2.36) to collectively deal with a series of vertex diagrams reduces the total task needed to prepare the integrals significantly. For instance, at the tenth order, there are

(Footnote 10 continued)
where the sum is taken over the lepton lines where an external photon vertex can be inserted in a self-energy-like diagram. $\widetilde{C}_{ij}$ is actually a homogeneous polynomial of degree n. We must deal with these $\widetilde{C}_{ij}$ in addition to U, B_{ij} and A_i.

6,354 quenched-type diagrams. Since nine vertex diagrams are related to each single quenched-type self-energy-like diagram, the WT-identity (2.36) thus reduces them to 706 self-energy-like diagrams. Time reflection invariance in QED further reduces the number of independent integrals to 389 [28].

We call the sum of the $g-2$ amplitudes over the set of vertex diagrams related via the WT-identity to a single self-energy-like diagram $\mathscr{G}$ as the *WT-summed amplitude*. The bare WT-summed amplitude, denoted by $M_{\mathscr{G}}$, in general contains infrared (IR) divergence(s). Therefore, the additional subtraction terms must be added to remove those IR divergences and to get the integral which can be carried out with a supercomputer system. Symbolically, such a finite integral takes the form

$$\Delta\mathscr{M}_{\mathscr{G}} = \int (dz)_{\mathscr{G}} \left(f_{\mathscr{G}}^{\text{bare}}(z) + \sum_{\mathfrak{F}} f_{\mathfrak{F}}^{\text{UV}}(z) + \sum_{\mathfrak{G}} f_{\mathfrak{G}}^{\text{IR}}(z) \right), \tag{2.53}$$

Each of UV subtraction terms necessary for the muon $g-2$ is in one-to-one correspondence with a normal forest $\mathfrak{F}$. A forest of a diagram $\mathscr{G}$ is a set of UV-divergent one-particle irreducible subdiagrams, any two of which are not overlapped with each other.[11] A forest is normal if it does not contain $\mathscr{G}$ as its element.

Before proceeding further, a comment on the necessity of IR subtraction is in order here. The sum of the on-mass-shell subtracted amplitudes over each gauge-invariant subset $\{\mathscr{G}\}'$, i.e.,

$$a_\psi\left(\{\mathscr{G}\}'\right) = \sum_{\{\mathscr{G}\}'} \left\{ M_{\mathscr{G}} + \sum_{\mathfrak{F}_{\mathscr{G}}} F_{\mathfrak{F}_{\mathscr{G}}}^{\text{UV, on-shell}} \right\}, \tag{2.54}$$

is finite. The expression on the right-hand side of Eq. (2.54) can be cast into the form required for the numerical subtraction

$$a_\psi\left(\{\mathscr{G}\}'\right) = \sum_{\{\mathscr{G}\}'} \int (dz)_{\mathscr{G}} \left\{ f_{\mathscr{G}}^{\text{bare}} + \sum_{\mathfrak{F}_{\mathscr{G}}} f_{\mathfrak{F}_{\mathscr{G}}}^{\text{UV, on-shell}} \right\}. \tag{2.55}$$

The essence of derivation of this form can be seen in the case where $\mathscr{G}$ have a vertex subdiagram $\mathscr{S}$, and focus on the forest $\mathfrak{F} = \{\mathscr{S}\}$, for simplicity. The on-mass-shell subtraction term corresponding to $\{\mathscr{S}\}$ is given by the product

$$F_{\{\mathscr{S}\}}^{\text{UV, on-shell}} = M_{\mathscr{G}/\mathscr{S}}\, L_{\mathscr{S}}\,, \tag{2.56}$$

of the vertex renormalization constant $L_{\mathscr{S}}$ on mass shells and the WT-summed magnetic moment $M_{\mathscr{G}/\mathscr{S}}$ of the reduced (self-energy-like) diagram $\mathscr{G}/\mathscr{S}$ which

[11] Two subdiagrams $\mathscr{S}_1$ and $\mathscr{S}_2$ are said to be *overlapped* if $\mathscr{S}_1 \cap \mathscr{S}_2 \neq \emptyset$, but neither $\mathscr{S}_1 \subset \mathscr{S}_2$ nor $\mathscr{S}_1 \supset \mathscr{S}_2$.

is obtained by shrinking $\mathscr{S}$ to a point-like vertex in $\mathscr{G}$. The parametric integral formalism allows to express $L_{\mathscr{S}}$ and $M_{\mathscr{G}/\mathscr{S}}$ as the integrals of *respective* sets of Feynman parameters. Thus, their product takes the form

$$M_{\mathscr{G}/\mathscr{S}}\, L_{\mathscr{S}} = \sum_{\alpha,\,\beta} \Gamma(\alpha) \int (dz)_{\mathscr{G}/\mathscr{S}} \frac{g_\alpha\,[\mathscr{G}/\mathscr{S}]}{\left(V_{\mathscr{G}/\mathscr{S}}\right)^\alpha} \times \Gamma(\beta) \int (dz)_{\mathscr{S}} \frac{g_\beta\,[\mathscr{S}]}{(V_{\mathscr{S}})^\beta}\,, \tag{2.57}$$

where, for instance, $g_\alpha[\mathscr{S}]$ is a function with equal numbers of $U_{\mathscr{S}}$, $B'^{\mathscr{S}}_{ij}$, $A^{\mathscr{S}}_i$. The application of the formula

$$\frac{\Gamma(\alpha)}{H^\alpha}\,\frac{\Gamma(\beta)}{K^\beta} = \Gamma(\alpha+\beta) \int_0^1 ds \int_0^1 dt\, \delta(1-s-t)\, \frac{s^{\alpha-1}\, t^{\beta-1}}{(sH+tK)^{\alpha+\beta}}\,, \tag{2.58}$$

and rescaling of the Feynman parameters will reduce Eq. (2.57) to the desired form [29]

$$M_{\mathscr{G}/\mathscr{S}}\, L_{\mathscr{S}} = \int (dz)_{\mathscr{G}} \sum_{\alpha,\,\beta} \Gamma(\alpha+\beta) \frac{g_\alpha\,[\mathscr{G}/\mathscr{S}]\; g_\beta\,[\mathscr{S}]}{\left(V_{\mathscr{G}/\mathscr{S}} + V_{\mathscr{S}}\right)^{\alpha+\beta}}\,. \tag{2.59}$$

The integrand on the right-hand side is exactly $f^{\text{UV, on-shell}}_{\{\mathscr{S}\}}$ in Eq. (2.55). By construction, the integral in Eq. (2.55) for each $\mathscr{G}$ is free from UV divergence. However, it contains IR subdivergence, in general. The form (2.55) demands that cancellation of IR subdivergence be realized when the summation is taken over $\{\mathscr{G}\}'$, not at the stage of integration. This implies that the form (2.55) may allow cancellation of UV divergence, but never does so for IR divergence *at the numerical level*. This is the reason why explicit construction of IR subtraction is necessary in the numerical approach.

In what follows, we will see the construction of UV subtraction terms first, and that of IR subtraction terms next.

We first concentrate on the construction of UV subtraction terms. As was stressed above, the numerical subtraction can be attained only if the subtraction terms are prepared on the same Feynman parameter space as the bare amplitude so that the UV singularities of the bare amplitude are cancelled in a pointwise way. As we have seen already above, the on-mass-shell subtraction term can be cast into such a required form, and the maximally contracted term involved in $L_{\mathscr{S}}$ in fact cancels the UV divergence. However, the on-shell subtraction term in general brings the additional IR divergence not present in the bare amplitude through non-maximally contracted terms. As discussed in the last paragraph in Sect. 2.4.2, lesser and lesser contracted terms tend to be dominated by the dynamics of degrees of freedom with longer and longer wavelength.

For this reason, renormalization is processed in two steps. That is, the UV subtraction terms $f^{\text{UV}}_{\mathfrak{F}}(z)$ in $\Delta\mathscr{M}_{\mathscr{G}}$ in Eq. (2.53) are constructed according to the *K operation* [27], which provides the UV subtraction term free from IR subdivergence. The second step, called the *residual renormalization*, calculates the difference between the

renormalization condition corresponding to K operation and the on-shell condition.[12] This step adds the finite term $R\left(\{\mathscr{G}\}'\right)$ to the sum of $\Delta\mathscr{M}_{\mathscr{G}}$ over a gauge-invariant subset $\{\mathscr{G}\}'$

$$a_{\psi}^{(2n)}\left(\{\mathscr{G}\}'\right) = \sum_{\{\mathscr{G}\}'} \Delta\mathscr{M}_{\mathscr{G}} + R\left(\{\mathscr{G}\}'\right). \tag{2.60}$$

To state the content of the K operation, we define the *UV limit*. For simplicity, we deal with the forest $\{\mathscr{S}\}$ consisting of a single vertex or self-energy subdiagram $\mathscr{S}$. We suppose that the Feynman parameters are organized to parametrize the corresponding UV singularity on the boundary $z_i \sim 0\,(i \in \mathscr{S})$. The UV limit $[A]^{\mathrm{UV}}_{\mathscr{S}}$ of the quantity A is defined to gather all the leading terms of ϵ ($\epsilon \ll 1$) for

$$z_j = \begin{cases} O(\epsilon) & \text{if } j \in \mathscr{S} \\ O(1) & \text{otherwise} \end{cases}. \tag{2.61}$$

Now, K operation is defined as the following manipulation *on the integrand*:

(1) It extracts only the maximally contracted terms.
(2) B_{ij}, A_j appearing in the numerator of the integrand and U are replaced by the corresponding UV limits.
(3) V is replaced by $V_{\mathscr{S}} + V_{\mathscr{R}}$, where $\mathscr{R}$ is the reduced diagram, and $V_{\mathscr{S}}$ and $V_{\mathscr{R}}$ are written in terms of Feynman parameters and scalar currents in $\mathscr{S}$ and $\mathscr{R}$, respectively.

(1) and (3), where V is not replaced by its UV limit, are necessary in order not to introduce any additional IR divergences.

The most important feature of the integral obtained via K operation is the factorization property; the subtraction terms obtained via K operation are given by the sum of the products of the quantities associated with the subdiagrams $\mathscr{S}_i$ of the forest $\{\mathscr{S}_i\}$ and the magnetic moment of the reduced self-energy-like diagram. Again, let's consider a forest $\{\mathscr{S}\}$ consisting of a single UV-divergent subdiagram. If $\mathscr{S}$ is a vertex subdiagram, $\mathscr{R} = \mathscr{G}/\mathscr{S}$ and

$$\mathsf{K}_{\mathscr{S}} M_{\mathscr{G}} = L^{\mathrm{UV}}_{\mathscr{S}}\, M_{\mathscr{G}/\mathscr{S}}\,, \tag{2.62}$$

where $L^{\mathrm{UV}}_{\mathscr{S}}$ denotes the maximally contracted terms of $L_{\mathscr{S}}$. If $\mathscr{S}$ is a self-energy subdiagram, the result of K operation consists of two terms

$$\mathsf{K}_{\mathscr{S}} M_{\mathscr{G}} = \delta m^{\mathrm{UV}}_{\mathscr{S}}\, M_{\mathscr{G}/\mathscr{S}(i^*)} + B^{\mathrm{UV}}_{\mathscr{S}}\, M_{\mathscr{G}/\{\mathscr{S},\, i\}}\,. \tag{2.63}$$

In $\mathscr{G}/\mathscr{S}(i^*)$, the remnant of $\mathscr{S}$ is left as the mass insertion vertex $(*)$ on a lepton line i connecting $\mathscr{S}$ to the rest of $\mathscr{G}$. Note that $\mathscr{G}/\mathscr{S}(i^*)$ and $\mathscr{G}/\{\mathscr{S},\, i\}$ have the same

[12] The masses of leptons and the electric charge can be used only for the amplitude renormalized in the on-shell renormalization condition.

chain topology so that $V_{\mathscr{G}/\{\mathscr{S},i\}}$ can be used in Sect. 2.4.3. The UV-finite amplitude $M^{\mathrm{R}}_{\mathscr{G}}$, which may contain IR divergence, is obtained from the forest formula with use of K operation

$$M^{\mathrm{R}}_{\mathscr{G}} = M_{\mathscr{G}} + \sum_{\mathfrak{F}} \prod_{\mathscr{S}\in\mathfrak{F}} (-\mathsf{K}_{\mathscr{S}})\, M_{\mathscr{G}}\,, \tag{2.64}$$

whose integral is organized in the same form as in Eq. (2.54).

Because the on-shell subtraction terms by definition exhibit the same factorization as above, the factorization property of K operation (and IR-subtraction scheme explained below) guarantees that *the residual renormalization term* $R\left(\{\mathscr{G}\}'\right)$ *in Eq.* (2.60) *can be written as the sum of the products of finite quantities at lower orders*. The factorization property of the amplitude obtained by K operation follows from the factorization of U, B_{ij} and A_i under the UV limit [27, 28].

Next, we turn our attention to the construction of IR-subtraction terms. The method we seek should be systematic enough to be implemented as a code to produce those terms as numerical programs.

IR subtraction is not as simple as UV subtraction in various respects. First, no general formula like Zimmermann's forest formula has been found. This may be due to the fact that IR subtraction is a tentatively required operation. The method to construct IR-subtraction terms must therefore be invented for the individual problems.

Another important difference from UV subtraction is that the IR singularities involved in the bare amplitude $M_{\mathscr{G}}$ can become harder than logarithmic. Indeed, there are eighth- and tenth-order diagrams that contain linear IR divergence. To recognize that the subtraction of such hard singularities is a complicated problem, we recall the fact that UV divergence is at most logarithmic at any order of perturbation. Thus, only leading singularity needs to be subtracted for UV. Indeed, this is attained by K operation, whose main part is composed of the power-counting operation, UV limit. However, if the quantity diverges linearly, the next-to-leading-order singularity must also be extracted from it. This is actually hard to do along the lines of any power-counting scheme. We thus have invented an IR-subtraction scheme for the high-order QED contribution to $g-2$, which is systematic enough to be implemented as the code generating numerical programs [29].

IR divergence arises basically in the following way. Let's consider the vertex diagram in Fig. 2.1 with the external leptons on their mass shells, $p_F^2 = m^2 = p_I^2$. The amplitude contains the IR-divergent piece which is proportional to

$$\begin{aligned}&\int \frac{d^4k}{k^2}\,\frac{1}{(k+p_F)^2-m^2}\,\frac{1}{(k+p_I)^2-m^2}\\ &\quad=\int \frac{d^4k}{k^2}\,\frac{1}{k^2+2p_F\cdot k}\,\frac{1}{k^2+2p_I\cdot k}\,.\end{aligned} \tag{2.65}$$

If a mass insertion vertex is inserted into one of the internal lepton lines in Fig. 2.1, IR divergence becomes harder. This indicates the mechanism of how worse IR divergence can arise at higher orders. That is, a diagram with more self-energy

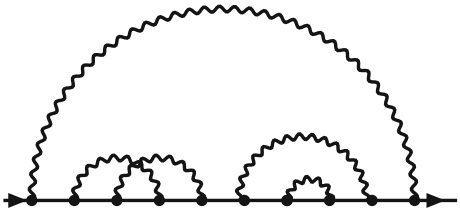

Fig. 2.9 A self-energy-like diagram having IR singularities which are logarithmic and harder at the tenth order

subdiagrams which are disconnected to one another can have harder IR divergence. Figure 2.9 illustrates such a self-energy-like diagram. The hardest IR divergence arises when only the outmost photon carries longer wavelength compared to the others and all the self-energy subdiagrams involved become relatively point-like.

One may imagine that the hard IR divergences arising through such a mechanism will be removed by the UV-subtraction terms corresponding to the self-energy diagrams. It is correct. But, as remarked at the stage of UV subtraction, full on-mass-shell renormalization can bring additional IR subdivergence through the wave function renormalization constant. For this reason, K operation is used for the construction of UV-subtraction terms. Suppose that the self-energy diagrams are all second-order. Then, the on-shell mass renormalization constant δm is equal to its UV limit δm^{UV}; $\delta m = \delta m^{\mathrm{UV}}$ and the amplitude which is made UV-finite by K operation becomes free from hard IR subdivergence. In general, in order to completely eliminate hard IR subdivergence, say for a forest consisting of a single self-energy subdiagram $\{\mathscr{S}\}$, it suffices to subtract the term in proportion to the difference $\delta m^{\mathrm{R}}_{\mathscr{S}} \equiv \delta m_{\mathscr{S}} - \delta m^{\mathrm{UV}}_{\mathscr{S}}$ − (all UV subdivergences) from the UV-finite amplitude $M^{\mathrm{R}}_{\mathscr{G}}$. This is exactly the idea of the R operation defined in [29]

$$\mathsf{R}_{\mathscr{S}} M^{\mathrm{R}}_{\mathscr{G}} \equiv M^{\mathrm{R}}_{\mathscr{G}/\mathscr{S}(i^*)}\, \delta m^{\mathrm{R}}_{\mathscr{S}}\,. \tag{2.66}$$

Equation (2.59) and its generalization to the product of more than two terms will convert the result of $\mathsf{R}_{\mathscr{S}} M^{\mathrm{R}}_{\mathscr{G}}$ into such a form of the integral that allows to cancel IR subdivergence in a pointwise way on the same Feynman parameter space as the bare amplitude.

The amplitude obtained by applying required R operations may be logarithmically divergent. They can be removed by I operation, say, for a single self-energy diagram $\mathscr{S}$ of a self-energy-like diagram $\mathscr{G}$ [29]

$$\mathsf{I}_{\mathscr{S}} M^{\mathrm{R}}_{\mathscr{G}} \equiv L^{\mathrm{R}}_{\mathscr{G}/\mathscr{S}(k)}\, M^{\mathrm{R}}_{\mathscr{S}}\,. \tag{2.67}$$

Here, $\mathscr{G}/\mathscr{S}(k)$ is obtained by inserting an external vertex k into one of the internal lepton lines in $\mathscr{S}$ which lies on the open path connected to the external leptons, and shrinking it to a point. $L^{\mathrm{R}}_{\mathscr{G}/\mathscr{S}(k)}$ is UV-finite but contains IR divergence; it is obtained by applying required K-operations to the on-mass-shell vertex renormalization constant $L_{\mathscr{G}/\mathscr{S}(k)}$.

The required IR-subtraction terms are characterized by the *annotated forests*. An annotated forest α is a set of pairs $(\mathscr{S}, \mathsf{O})$ of a self-energy subdiagram $\mathscr{S}$ of a self-energy-like diagram $\mathscr{G}$ and the operation $\mathsf{O} = \mathsf{R}$ or I with one restriction; if $\mathscr{S}_1 \subset \mathscr{S}_2$, $(\mathscr{S}_1, \mathsf{I})$ and $(\mathscr{S}_2, \mathsf{R})$ are prohibited as the elements of an annotated forest. If $\mathfrak{A}$ denotes the set of all normal annotated forests, the finite amplitude $\Delta M_{\mathscr{G}}$ is obtained as

$$\Delta M_{\mathscr{G}} = M^{\mathsf{R}}_{\mathscr{G}} + \sum_{\alpha \in \mathfrak{A}} \prod_{(\mathscr{S}, \mathsf{O}) \in \alpha} (-\mathsf{O}_{\mathscr{S}})\, M^{\mathsf{R}}_{\mathscr{G}}\,, \tag{2.68}$$

where, if $\mathscr{S}_1 \subset \mathscr{S}_2$, the operators act according to the following order

(i) $\mathsf{R}_{\mathscr{S}_2}\, \mathsf{R}_{\mathscr{S}_1}$.
(ii) $\mathsf{I}_{\mathscr{S}_1}\, \mathsf{I}_{\mathscr{S}_2}$.
(iii) $\mathsf{R}_{\mathscr{S}_1}\, \mathsf{I}_{\mathscr{S}_2}$.

2.5 Result for QED Contribution

By combining Eqs. (2.5) with (2.27), a_e is found to be represented as a power series with respect to the fine structure constant α

$$a_e(\alpha) = \text{non-QED contribution} + \sum_{n=1}^{\infty} a_e^{(2n)} \left(\frac{\alpha}{\pi}\right)^n . \tag{2.69}$$

Table 2.2 implies that the theoretical ambiguity in the "non-QED contribution" is less than the experimental uncertainty of a_e, but cannot be negligible. Therefore, if the relevant coefficients $a_e^{(2n)}$ in the perturbative expansion of the QED contribution can be computed with sufficient precision, equating such obtained $a_e(\alpha)$ as a function of α to the experimental value $a_e(\text{exp})$ will yield the value of α, referred to as $\alpha(a_e)$.

Table 2.3 summarizes the terms $A_j^{(2n)}$ in each coefficients $a_e^{(2n)}$ of $a_e(\text{QED})$. See Eq. (2.29) for the definition of $A_j^{(2n)}$. $A_1^{(2)}$ [4], $A_1^{(4)}$ [30, 31], and $A_1^{(6)}$ [32] are known exactly. We also have the analytic expression for $A_2^{(2)}$ [33], $A_2^{(4)}$ [34, 35] and the asymptotic expansion in mass ratios for $A_3^{(6)}$ [36, 37]. The uncertainties of these terms are attributed to the ones in lepton mass ratios. The values in Table 2.3 were recalculated using the newest values [38].

$$\begin{aligned}
\frac{m_e}{m_\mu} &= 4.83633166\ (12) \times 10^{-3}\,, \\
\frac{m_e}{m_\tau} &= 2.87592\ (26) \times 10^{-4}\,, \\
\frac{m_\mu}{m_\tau} &= 5.94649\ (54) \times 10^{-2}\,.
\end{aligned} \tag{2.70}$$

All of $A_j^{(8)}$ and $A_j^{(10)}$ have been obtained only by the numerical means explained in Sect. 2.4.

From Table 2.3, we can explicitly see that the mass-independent term $A_1^{(2n)}$ dominates the coefficient $a_e^{(2n)}$ of the perturbative expansion of the QED contribution to the electron $g-2$, and the orders of magnitude of them are all unity.

Now, by using the result in Table 2.3 for $a_e^{(2n)}$ in Eq. (2.69), we get [39]

$$\alpha^{-1}(a_e) = 137.035\,999\,1727\,(68)_{8\text{th}}(46)_{10\text{th}}(19)_{\text{QCD}}(331)_{\text{exp}}\,, \tag{2.71}$$

where the uncertainties come from the eighth-order QED coefficient $a_e^{(8)}$, the tenth-order coefficient $a_e^{(10)}$, the QCD contribution, and the experiment (2.3) of the electron $g-2$, respectively.

Recall that the value of α has also been determined by various other methods such as quantum Hall effect, etc [38, 40]. In particular, besides the electron $g-2$, the precise α has been obtained by determination of the ratio h/m_A due to the atom recoil-velocity measurement for $A =$ cesium [41] and $A =$ rubidium [42] combined with the Rydberg constant and m_{Rb}/m_e in [38]

$$\alpha^{-1}(\text{Rb}) = 137.035\,999\,049\,(90)\,. \tag{2.72}$$

Within the present precision, Eq. (2.71) is compatible with Eq. (2.72)

$$\alpha^{-1}(a_e) - \alpha^{-1}(\text{Rb}) = 124(96)\times 10^{-9}\,. \tag{2.73}$$

In this way, check of consistency of the values of α thus obtained provides us a cross-sectional understanding on wide range of physical phenomena.

Instead, if we use the value (2.72) for the fine structure constant, we obtain the following prediction for $a_e(\text{SM})$

Table 2.3 The terms $A_j^{(2n)}$ in the coefficients $a_e^{(2n)}$

$2n$	$A_1^{(2n)}$	$A_2^{(2n)}\left(\frac{m_e}{m_\mu}\right)$	$A_2^{(2n)}\left(\frac{m_e}{m_\tau}\right)$	$A_3^{(2n)}\left(\frac{m_e}{m_\mu}, \frac{m_e}{m_\tau}\right)$
2	0.5	–	–	–
4	−0.328478965579...	$5.19738667\,(26)\times 10^{-7}$	$1.83798\,(34)\times 10^{-9}$	–
6	1.181241456...	$-7.37394155\,(27)\times 10^{-6}$	$-6.5830\,(11)\times 10^{-8}$	$0.1909\,(1)\times 10^{-12}$
8	−1.9106 (20)	$9.222\,(66)\times 10^{-4}$	$8.24\,(12)\times 10^{-6}$	$7.465\,(18)\times 10^{-7}$
10	9.168 (571)	−0.00382 (39)	◇	◇

There are no Feynman diagrams for $A_2^{(2)}\left(\frac{m_e}{m_\mu}\right)$, $A_2^{(2)}\left(\frac{m_e}{m_\tau}\right)$ and $A_3^{(2n)}\left(\frac{m_e}{m_\mu}, \frac{m_e}{m_\tau}\right)$ $(2n = 2,\ 4)$.

$A_2^{(10)}\left(\frac{m_e}{m_\tau}\right)$ and $A_3^{(10)}\left(\frac{m_e}{m_\mu}, \frac{m_e}{m_\tau}\right)$ have not been computed as they are much smaller than $A_2^{(10)}\left(\frac{m_e}{m_\mu}\right)$, and is thus negligible for the precision of our interest

$$a_e(\mathrm{SM},\ \mathrm{Rb}) = 1\ 159\ 652\ 180.07\ (6)_{8\mathrm{th}}(8)_{10\mathrm{th}}(3)_{\mathrm{QCD}}(77)_{\alpha(\mathrm{Rb})} \times 10^{-12}\,. \quad (2.74)$$

The comparison of this with Eq. (2.3) is less impressive due to the uncertainty of $\alpha^{-1}(\mathrm{Rb})$.

Acknowledgments The author thanks T. Aoyama, T. Kinoshita and M. Nio for the collaboration over a long period of time, and K. Asano and N. Watanabe for their intensive works in the short term. The numerical integration of the eighth and tenth order contribution has been carried out using supercomputer systems, RSCC and RICC. This work is supported in part by the JSPS Grant-in-Aid for Scientific Research (C)20540261.

References

1. D. Hanneke, S. Fogwell, G. Gabrielse, New measurement of the electron magnetic moment and the fine structure constant. Phys. Rev. Lett. **100**, 120801 (2008). doi:DOIurl10.1103/PhysRevLett.100.120801
2. D. Hanneke, S. Fogwell Hoogerheide, G. Gabrielse, Cavity control of a single-electron quantum cyclotron: measuring the electron magnetic moment. Phys. Rev. A **83**, 052122 (2011)
3. R. Van Dyck, P. Schwinberg, H. Dehmelt, New high-precision comparison of electron and positron g-factors. Phys. Rev. Lett. **59**, 26 (1987). doi:10.1103/PhysRevLett.59.26
4. J.S. Schwinger, On quantum-electrodynamics and the magnetic moment of the electron. Phys. Rev. **73**, 416 (1948). doi:10.1103/PhysRev.73.416
5. G. 't Hooft, M. Veltman, Regularization and renormalization of gauge fields. Nucl. Phys. **B44**, 189 (1972). doi:10.1016/0550-3213(72)90279-9
6. R. Feynman, Space-time approach to quantum electrodynamics. Phys. Rev. **76**, 769 (1949). doi:10.1103/PhysRev.76.769
7. F. Jegerlehner, A. Nyffeler, The muon $g-2$. Phys. Rep. **477**, 1 (2009). doi:10.1016/j.physrep.2009.04.003
8. K. Hagiwara, A. Martin, D. Nomura, T. Teubner, Predictions for $g-2$ of the muon and $\alpha_{QED}(M_Z^2)$. Phys. Rev. **D69**, 093003 (2004). doi:10.1103/PhysRevD.69.093003
9. D. Nomura, T. Teubner, Hadronic contributions to the anomalous magnetic moment of the electron and the hyperfine splitting of muonium. Nucl. Phys. **B867**, 236 (2013). doi:10.1016/j.nuclphysb.2012.10.001
10. J. Prades, E. de Rafael, A. Vainshtein, in *Hadronic Light-by-Light Scattering Contribution to the Muon Anomalous Magnetic Moment*. ed. by B. Lee Roberts, William J. Marciano. Lepton Dipole Moments (Advanced Series on Directions in High Energy Physics), vol 20 (World Scientific, Singapore, 2009)
11. K. Fujikawa, B. Lee, A. Sanda, Generalized renormalizable Gauge formulation of spontaneously broken Gauge theories. Phys. Rev. **D6**, 1972 (2923). doi:10.1103/PhysRevD.6.2923
12. A. Czarnecki, B. Krause, W.J. Marciano. Electroweak corrections to the muon anomalous magnetic moment. Phys. Rev. Lett. **76**, 3267 (1996). doi:10.1103/PhysRevLett.76.3267
13. M. Knecht, S. Peris, M. Perrottet, E. De Rafael, Electroweak hadronic contributions to the muon $(g-2)$. JHEP **0211**, 003 (2002)
14. A. Czarnecki, W.J. Marciano, A. Vainshtein, Refinements in electroweak contributions to the muon anomalous magnetic moment. Phys. Rev. **D67**, 073006 (2003). doi:10.1103/PhysRevD.67.073006, doi:10.1103/PhysRevD.73.119901
15. T. Kinoshita, M. Nio, Tenth-order QED contribution to the lepton $g-2$: evaluation of dominant α^5 terms of muon $g-2$. Phys. Rev. **D73**, 053007 (2006). doi:10.1103/PhysRevD.73.053007
16. T. Aoyama, M. Hayakawa, T. Kinoshita, M. Nio, N. Watanabe, Eighth-order vacuum-polarization function formed by two light-by-light-scattering diagrams and its contribution to

the tenth-order electron $g-2$. Phys. Rev. **D78**, 053005 (2008). doi:10.1103/PhysRevD.78.053005
17. T. Aoyama, M. Hayakawa, T. Kinoshita, M. Nio, Tenth-order lepton anomalous magnetic moment: Second-order vertex containing two vacuum polarization subdiagrams, one within the other. Phys. Rev. **D78**, 113006 (2008). doi:10.1103/PhysRevD.78.113006
18. T. Aoyama, K. Asano, M. Hayakawa, T. Kinoshita, M. Nio, et al., Tenth-order lepton $g-2$: contribution from diagrams containing sixth-order light-by-light-scattering subdiagram internally. Phys. Rev. **D81**, 053009 (2010). doi:10.1103/PhysRevD.81.053009
19. T. Aoyama, M. Hayakawa, T. Kinoshita, M. Nio, Tenth-order lepton $g-2$: contribution of some fourth-order radiative corrections to the sixth-order $g-2$ containing light-by-light-scattering subdiagrams. Phys. Rev. **D82**, 113004 (2010). doi:10.1103/PhysRevD.82.113004
20. T. Aoyama, M. Hayakawa, T. Kinoshita, M. Nio, Proper eighth-order vacuum-polarization function and its contribution to the tenth-order lepton $g-2$. Phys. Rev. **D83**, 053003 (2011). doi:10.1103/PhysRevD.83.053003
21. T. Aoyama, M. Hayakawa, T. Kinoshita, M. Nio, Tenth-order QED contribution to lepton anomalous magnetic moment: fourth-order vertices containing sixth-order vacuum-polarization subdiagrams. Phys. Rev. **D83**, 053002 (2011). doi:10.1103/PhysRevD.83.053002
22. T. Aoyama, M. Hayakawa, T. Kinoshita, M. Nio, Tenth-order lepton anomalous magnetic moment sixth-order vertices containing vacuum-polarization subdiagrams. Phys. Rev. **D84**, 053003 (2011). doi:10.1103/PhysRevD.84.053003
23. T. Aoyama, M. Hayakawa, T. Kinoshita, M. Nio, Tenth-order QED lepton anomalous magnetic moment: eighth-order vertices containing a second-order vacuum polarization. Phys. Rev. **D85**, 033007 (2012). doi:10.1103/PhysRevD.85.033007
24. T. Aoyama, M. Hayakawa, T. Kinoshita, M. Nio, Tenth-order QED contribution to the lepton anomalous magnetic moment: sixth-order vertices containing an internal light-by-light-scattering subdiagram. Phys. Rev. **D85**, 093013 (2012). doi:10.1103/PhysRevD.85.093013
25. T. Aoyama, M. Hayakawa, T. Kinoshita, M. Nio, Quantum electrodynamics calculation of lepton anomalous magnetic moments: Numerical approach to the perturbation theory of QED. Prog. Theor. Exp. Phys. **2012**, 01A107 (2012). doi:10.1093/ptep/pts030
26. P. Cvitanovic, T. Kinoshita, Feynman-Dyson rules in parametric space. Phys. Rev. **D10**, 3978 (1974). doi:10.1103/PhysRevD.10.3978
27. P. Cvitanovic, T. Kinoshita, New approach to the separation of ultraviolet and infrared divergences of Feynman-parametric integrals. Phys. Rev. **D10**, 3991 (1974). doi:10.1103/PhysRevD.10.3991
28. T. Aoyama, M. Hayakawa, T. Kinoshita, M. Nio, Automated calculation scheme for α^n contributions of QED to lepton $g-2$: generating renormalized amplitudes for diagrams without lepton loops. Nucl. Phys. **B740**, 138 (2006). doi:10.1016/j.nuclphysb.2006.01.040
29. T. Aoyama, M. Hayakawa, T. Kinoshita, M. Nio, Automated calculation scheme for α^n contributions of QED to lepton g-2: new treatment of infrared divergence for diagrams without lepton loops. Nucl. Phys. **B796**, 184 (2008). doi:10.1016/j.nuclphysb.2007.12.013
30. A. Petermann, Fourth-order magnetic moment of the electron. Helv. Phys. Acta **30**, 407 (1957)
31. C.M. Sommerfield, Magnetic dipole moment of the electron. Phys. Rev. **107**, 328 (1957). doi:10.1103/PhysRev.107.328
32. S. Laporta, E. Remiddi, The analytical value of the electron $(g-2)$ at order α^3 in QED. Phys. Lett. B379, **283** (1996). doi:10.1016/0370-2693(96)00439-X
33. H. Elend, On the anomalous magnetic moment of the muon. Phys. Lett. 20, **682** (1966). doi:10.1016/0031-9163(66)91171-1. Erratum: ibid., **21**, 720 (1966)
34. S. Laporta, E. Remiddi, The analytical value of the electron light-light graphs contribution to the muon $(g-2)$ in QED. Phys. Lett. **B301**, 440 (1993). doi:10.1016/0370-2693(93)91176-N
35. S. Laporta, The analytical contribution of the sixth-order graphs with vacuum polarization insertions to the muon $(g-2)$ in QED. Nuovo Cim. **A106**, 675 (1993). doi:10.1007/BF02787236

36. A. Czarnecki, M. Skrzypek, The muon anomalous magnetic moment in QED: three-loop electron and tau contributions. Phys. Lett. **B449**, 354 (1999). doi:10.1016/S0370-2693(99)00076-3
37. S. Friot, D. Greynat, E. De Rafael, Asymptotics of Feynman diagrams and the Mellin Barnes representation. Phys. Lett. **B628**, 73 (2005). doi:10.1016/j.physletb.2005.08.126
38. Rev. Mod. Phys. CODATA recommended values of the fundamental physical constants: 2010. **84**(1527), 2012 (2010). doi:10.1103/RevModPhys.84.1527
39. T. Aoyama, M. Hayakawa, T. Kinoshita, M. Nio, Tenth-order QED contribution to the electron $g-2$ and an improved value of the fine structure constant. Phys. Rev. Lett. **109**, 111807 (2012). doi:10.1103/PhysRevLett.109.111807.
40. T. Kinoshita, The fine structure constant. Rept. Prog. Phys. **59**, 1459 (1996). doi:10.1088/0034-4885/59/11/003.
41. A. Wicht, J.M. Hensley, E. Sarajlic, S. Chu, A preliminary measurement of the fine structure constant based on atom interferometry. Physica Scripta **T106**, 82 (2002). doi:10.1238/Physica.Topical.102a00082
42. R. Bouchendira, P. Clade, S. Guellati-Khelifa, F. Nez, F. Biraben, New determination of the fine structure constant and test of the quantum electrodynamics. Phys. Rev. Lett. **106**, 080801 (2011). doi:10.1103/PhysRevLett.106.080801

http://www.springer.com/978-3-642-45200-0

Fundamental Physics in Particle Traps
Quint, W.; Vogel, M. (Eds.)
2014, XXI, 411 p. 166 illus., Hardcover
ISBN: 978-3-642-45200-0